

Searching for the Flavon in the diphoton channel at future super hadron colliders.

M. A. Arroyo-Ureña,^{1,2,*} Diego Carreño,^{1,†} and T.A. Valencia-Pérez^{3,‡}

¹*Facultad de Ciencias Físico-Matemáticas,
Benemérita Universidad Autónoma de Puebla,
C.P. 72570, Puebla, Pue., México.*

²*Centro Interdisciplinario de Investigación y Enseñanza de la Ciencia,
Benemérita Universidad Autónoma de Puebla,
C.P. 72570, Puebla, Pue., México.*

³*Instituto de Física, Universidad Nacional Autónoma de México, C.P. 01000, CDMX, México.*

Abstract

We study the production of a CP-even flavon H_F in proton-proton collisions and the prospects for its detection via the diphoton channel at future super hadron colliders, i.e., $pp \rightarrow H_F \rightarrow \gamma\gamma$. The theoretical framework adopted is a model that invokes the Froggatt-Nielsen mechanism with an Abelian flavor symmetry, which includes a Higgs doublet and a complex singlet. We confront the free parameters of the model against theoretical and experimental constraints to find the allowed parameter space, which is then used to evaluate the production cross section of the flavon and the branching ratio of its decay into two photons. We find promising results based on specific benchmark points, achieving *signal significances* at the level of 5σ for flavon masses in the interval $200 \lesssim M_{H_F} \lesssim 450$ and integrated luminosities in the range $5 - 12 \text{ ab}^{-1}$ at the future High-Energy LHC. On the other hand, the Future hadron-hadron Circular Collider could probe masses up to 1 TeV if it reaches an integrated luminosity of at least 2 ab^{-1} .

* marco.arroyo@fcfm.buap.mx

† diego.carrenod@alumno.buap.mx

‡ tvalencia@fisica.unam.mx

I. INTRODUCTION

The Standard Model (SM) of particle physics [1–4] has been tested over the last five decades and has been shown to successfully describe elementary particle interactions, including the mechanism responsible for breaking electroweak symmetry [5–10]. This mechanism gives mass to the massive particles of the SM and predicts the existence of the Higgs boson (h). It was verified at LHC in the year 2012 at LHC [11, 12]. The CMS and ATLAS collaborations reported an excess of events from their datasets of proton-proton collisions at center-of-mass energy $\sqrt{s} = 7$ TeV in the mass region of 124-126 GeV at levels of 2.9 and 3.1σ , respectively. The searches were focused on different channels, that is, $h \rightarrow ZZ^* \rightarrow 4\ell$, $h \rightarrow WW^* \rightarrow e\nu\mu\nu$, $h \rightarrow \gamma\gamma$. Later, with a significance of 5.9σ the Higgs boson was observed at a centre-of-mass energy $\sqrt{s} = 8$ TeV, and it shown to be compatible with the prediction of the SM, being the last elementary particle discovered within the theoretical framework of the SM, proving to be a successful theory. However, it is well known that SM cannot help us understand some phenomena such as the nature of dark matter, the mass hierarchy problem, the flavor problem, etc. Thus, it is plausible to think that the SM is a limiting case of a more general theory, in this sense the SM can be considered as an effective theory valid at a certain energy scale. It is also reasonable to extend the SM motivated by possible answers to the open problems of the SM. There are a plethora of extensions that attempt to explain one or more of the open questions [], one possibility is the Froggatt-Nielsen mechanism [13] which attempts to explain the hierarchy of fermion masses. This mechanism assumes that above some scale Λ_F there is a symmetry, perhaps of Abelian type $U(1)_F$ (with the SM fermions being charged under it), which prohibits the emergence of Yukawa couplings at the renormalizable level. Yukawa matrices can arise through non-renormalizable operators, though. It is also reasonable to inquire whether hypothetical heavy Higgs bosons, as predicted by the Froggatt-Nielsen plus a complex singlet model (FNSM) [14], could be detected in the gold channels, namely, $H_F \rightarrow ZZ$, $H_F \rightarrow WW$, $H_F \rightarrow \gamma\gamma$, where H_F is the so-called *Flavon*. The $H_F \rightarrow ZZ$ and $H_F \rightarrow WW$ channels have already been really studied in [15]. However, to our knowledge, the di-photon channel has not yet been explored. This may be due to the suppression of the $H \rightarrow \gamma\gamma$ decay rate. Nevertheless, it has the advantages of good resolution on the Flavon mass M_{H_F} and small QCD backgrounds. A comprehensive study on the search for *Flavons* by considering $\mathcal{Z}_N \times \mathcal{Z}_M$ flavor symmetries is reported in [16], while the *Flavon* associated with dark matter is studied in [17].

In this paper, we are interested in the possible detection of the Flavon via the di-photon channel. Such a hypothetical particle is predicted in the FNSM, theoretical framework adopted in this investigation. The study is focused on future proton-proton pp colliders, namely:

- High-Luminosity Large Hadron Collider (HL-LHC) [18]. The HL-LHC is a new stage of the LHC starting about 2026 at center-of-mass energy of 14 TeV. The upgrade aims at increasing the integrated luminosity by a factor of ten (3 ab^{-1} , year 2035) with respect to the final stage

of the LHC (300 fb^{-1}).

- High-Energy Large Hadron Collider [19]. The HE-LHC is a possible future project at CERN. The HE-LHC will be a 27 TeV pp collider being developed for the 100 TeV Future Circular Collider. This project is designed to reach up to 12 ab^{-1} which opens a large window for new physics research.
- Future Circular hadron-hadron Collider [20]. The FCC-hh is a future 100 TeV pp hadron collider which will be able to discover rare processes, new interactions up to masses of around 30 TeV and search for a possible substructure of the quarks. Because the high energy and collision rate, up to 10^5 flavons may be produced. The FCC-hh will reach up to an integrated luminosity of 30 ab^{-1} in its final stage.

This work is structured as follows. In Sec. II, we conduct a comprehensive review of the FNSM. Experimental and theoretical constraints on the model parameter space are also included. Section III focuses on taking advantage of the insights gained from previous section, performing a computational analysis of the proposed signal and its SM background processes. Finally, the conclusions are presented in Sec. IV.

II. THEORETICAL FRAMEWORK

In this section we present the relevant theoretical aspects of the FNSM. In Refs.[] a deep theoretical analysis of the model and a study on the model parameter space are reported.

A. Scalar sector

The scalar sector includes one singlet complex scalar S_F to the SM. In the unitary gauge, the SM Higgs doublet Φ and S_F are written as follows,

$$\Phi = \begin{pmatrix} 0 \\ \frac{v+\phi^0}{\sqrt{2}} \end{pmatrix}, \quad S_F = \left(\frac{v_s + S_R + iS_I}{\sqrt{2}} \right),$$

where v_s and v stand for the VEVs of the complex singlet S_F and the SM Higgs doublet, respectively. The scalar potential is expected to be invariant under a flavor symmetry $U(1)_F$, which states that $\Phi \rightarrow \Phi$ and $S_F \rightarrow e^{i\alpha} S_F$. In general, the FNSM scalar potential allows for complex VEV $\langle S_F \rangle_0 = \frac{v_s}{\sqrt{2}} e^{i\xi}$. In this work, we consider the special case of CP-conserving *i.e.*, $\xi = 0$.

The CP-conserving scalar potential is then given by:

$$V_0 = -\frac{1}{2}m_1^2\Phi^\dagger\Phi - \frac{1}{2}m_2^2S_F^*S_F + \frac{1}{2}\lambda_1(\Phi^\dagger\Phi)^2 + \lambda_2(S_F^*S_F)^2 + \lambda_3(\Phi^\dagger\Phi)(S_F^*S_F). \quad (2.1)$$

After the spontaneous symmetry breaking by the VEVs of the scalar fields Φ and S_F , the massless Goldstone boson arises. To generate mass to it, we introduce a soft $U(1)_F$ breaking term to the scalar potential in Eq. (2.1):

$$V_{\text{soft}} = -\frac{1}{2}m_3^2(S_F^2 + S_F^{*2}). \quad (2.2)$$

Then, the complete scalar potential is given by:

$$V_{FNSM} = V_0 + V_{\text{soft}} \quad (2.3)$$

After both the SSB and the minimization conditions on the potential V_{FNSM} are performed, we identify a mixing between the spin-0 fields via the λ_3 parameter, which contributes to the mass terms as follows:

$$m_1^2 = v^2\lambda_1 + v_s^2\lambda_3, \quad (2.4)$$

$$m_2^2 = -2m_3^2 + 2v_s^2\lambda_2 + v^2\lambda_3. \quad (2.5)$$

Meanwhile, the soft $U(1)_F$ flavor symmetry-breaking term V_{soft} generates a pseudo-scalar Flavon mass.

Because all the parameters in the potential (2.1) are real, the imaginary and real parts of V_{FNSM} do not mix. The CP-even mass matrix written in the (ϕ_0, S_R) basis is given by

$$M_S^2 = \begin{pmatrix} \lambda_1 v^2 & \lambda_3 v v_s \\ \lambda_3 v v_s & 2\lambda_2 v_s^2 \end{pmatrix}$$

The mass eigenstates are obtained through the standard 2×2 rotation:

$$\begin{pmatrix} \phi^0 \\ S_R \end{pmatrix} = \begin{pmatrix} \cos \alpha & \sin \alpha \\ -\sin \alpha & \cos \alpha \end{pmatrix} \begin{pmatrix} h \\ H_F \end{pmatrix},$$

where we identify to h as the SM-like Higgs boson and H_F is the CP-even Flavon. The CP-odd Flavon is associated with the imaginary part of the complex singlet: $S_I \equiv A_F$ with mass $M_{A_F} = 2m_3^2$. The physical masses M_ϕ ($\phi = h, H_F, A_F$) are related to the parameters of the scalar potential in Eq.(2.1) as follows:

$$\lambda_1 = \frac{(\cos \alpha M_h)^2 + (\sin \alpha M_{H_F})^2}{v^2},$$

$$\lambda_2 = \frac{M_{A_F}^2 + (\cos \alpha M_{H_F})^2 + (\sin \alpha M_h)^2}{2v_s^2}, \quad (2.6)$$

$$\lambda_3 = \frac{\cos \alpha \sin \alpha}{vv_s} (M_{H_F}^2 - M_h^2).$$

B. Yukawa Lagrangian

The $U(1)_F$ invariant Yukawa Lagrangian is given by [13]:

$$\mathcal{L}_Y = \rho_{ij}^d \left(\frac{S_F}{\Lambda_F} \right)^{q_{ij}^d} \bar{Q}_i d_j \tilde{\Phi} + \rho_{ij}^u \left(\frac{S_F}{\Lambda_F} \right)^{q_{ij}^u} \bar{Q}_i u_j \Phi + \rho_{ij}^\ell \left(\frac{S_F}{\Lambda_F} \right)^{q_{ij}^\ell} \bar{L}_i \ell_j \Phi + \text{h.c.},$$

where ρ_{ij}^f ($f = u, d, \ell$) are dimensionless parameters of order $\mathcal{O}(1)$, q_{ij}^f is associated with to Abelian charges such as they reproduce the observed fermion masses, Λ is identified as the ultraviolet mass scale. The Yukawa couplings from Lagrangian (2.7) can be generated after spontaneously breaking the $U(1)_F$ and EW symmetries. By considering the unitary gauge and making the expansion of the neutral component of the heavy Flavon S_F around its VEV v_s , one obtains:

$$\left(\frac{S_F}{\Lambda_F} \right)^{q_{ij}} \simeq \left(\frac{v_s}{\sqrt{2}\Lambda_F} \right)^{q_{ij}} \left[1 + q_{ij} \left(\frac{S_R + iS_I}{v_s} \right) \right], \quad (2.7)$$

From Eqs. (2.7), (2.7) and after replacing the mass eigenstates, the Yukawa Lagrangian reads:

$$\begin{aligned} \mathcal{L}_Y &= \frac{1}{v} [\bar{U} M^u U + \bar{D} M^d D + \bar{L} M^\ell L] (c_\alpha h + s_\alpha H_F) \\ &+ \frac{v}{\sqrt{2}v_s} [\bar{U}_i \tilde{Z}_{ij}^u U_j + \bar{D}_i \tilde{Z}_{ij}^d D_j + \bar{L}_i \tilde{Z}_{ij}^\ell L_j] \\ &\times (-\sin \alpha h + \cos \alpha H_F + iA_F) + \text{h.c.}, \end{aligned} \quad (2.8)$$

where the Higgs-Flavon couplings are encapsulated in the $\tilde{Z}_{ij}^f = U_L^f Z_{ij}^f U_L^{f\dagger}$ matrix elements and M^f corresponds to the diagonal fermion mass matrix. In the flavor basis, the Z_{ij}^f is given by

$$Z_{ij}^f = \rho_{ij}^f \left(\frac{v_s}{\sqrt{2}\Lambda_F} \right)^{q_{ij}^f} q_{ij}^f. \quad (2.9)$$

Equation (2.9) remains nondiagonal even after process of diagonalization of the mass matrices, as a consequence the FNSM allows for flavor-changing neutral currents. From the kinetic terms of the Higgs doublet and the complex singlet we can extract the ϕVV ($V = W, Z$) interactions. Thus, we present the relevant Feynman rules in Table I.

Vertex (ϕXX)	Coupling constant ($g_{\phi XX}$)
$hf_i\bar{f}_j$	$\frac{c_\alpha}{v}\tilde{M}_{ij}^f - s_\alpha r_s \tilde{Z}_{ij}^f$
$H_F f_i \bar{f}_j$	$\frac{s_\alpha}{v}\tilde{M}_{ij}^f + c_\alpha r_s \tilde{Z}_{ij}^f$
$A_F f_i \bar{f}_j$	$r_s \tilde{Z}_{ij}^f$
hZZ	$\frac{g_{MZ}}{c_W} c_\alpha$
hWW	$gM_W c_\alpha$
$H_F ZZ$	$g\frac{M_Z}{c_W} s_\alpha$
$H_F WW$	$gM_W s_\alpha$

TABLE I: Tree-level couplings of the SM-like Higgs boson h and the Flavons H_F and A_F to fermion and gauge boson pairs in the FNSM. Here, $r_s = v/(\sqrt{2}v_s)$.

C. Model parameter space

In order to have realistic predictions, in this section we present a detailed analysis on the model parameter space. We mainly focus on the parameters that have a direct impact on the observable studied, *i.e.*, the production cross section of the Flavon and its subsequent decay into photons. According to Eqs. (3.4)-(3.6) we require constraining the following free parameters:

1. Cosine of the mixing angle α and
2. Vacuum expectation value of the complex singlet S_F : v_s .

The observables to constrain them include both theoretical and experimental constraints as follows.

Theoretical constraints

1. Stability of the scalar potential

The scalar potential in Eq. (2.1) requires absolute stability, *i.e.*, it should not become unbounded from below. The absolute stability demands the following conditions [21]

$$\lambda_{1,2}(\lambda) > 0, \quad \lambda_3(\Lambda) + \sqrt{2\lambda_1(\Lambda)\lambda_2(\Lambda)} > 0. \quad (2.10)$$

These potential parameters are evaluated at a scale Λ using Renormalization Group Evolution equations (RGE).

TABLE II: Parameters and ranges scanned.

Parameter	Range
v_s (GeV)	[0.001 – 5000]
M_{H_F} (GeV)	200 – 1000
M_{A_F} (GeV)	200 – 1000

2. *Perturbativity and unitarity constraints*

We also need to make sure that radiative corrections for the scalar potential remains perturbative at any given energy scale. To ensure this, one must impose upper bounds on the quartic couplings as follows:

$$|\lambda_{1,2,3}(\Lambda)| \leq 4\pi. \quad (2.11)$$

The quartic couplings are also severely constrained by the unitarity of the S-matrix, which demands that the eigenvalues of it should be less than 8π [21]. Using the equivalence theorem, the unitary bounds obtained from the S-matrix are given by:

$$\lambda_1(\Lambda) \leq 16\pi, \quad |\lambda_1(\Lambda) + \lambda_2(\Lambda) \pm \sqrt{(\lambda_1(\Lambda) - \lambda_2(\Lambda))^2 + ((2/3)\lambda_3(\Lambda))^2}| \leq 16\pi/3. \quad (2.12)$$

From conditions (2.10), (2.11), (2.11) and Eqs. (2.6), we can constrain the VEV v_s and the CP-even, CP-odd Flavons masses M_{H_F} , M_{A_F} . According our analysis, these theoretical constraints impose lower limits on the parameter v_s . We scanned over the parameters above aforementioned, the ranges studied are presented in Table II. Meanwhile, we present in Fig. 1 the $\cos \alpha - v_s$ plane. Blue points correspond to these allowed by all the theoretical constraints, being the unitarity restriction $|\lambda_1(\Lambda) + \lambda_2(\Lambda) + \sqrt{(\lambda_1(\Lambda) - \lambda_2(\Lambda))^2 + ((2/3)\lambda_3(\Lambda))^2}| \leq 16\pi/3$ the most stringent. We present values for v_s in the $[0, 200]$ interval because the theoretical constraints do not impose upper bounds on v_s .

Experimental constraints

3. *LHC Higgs boson data and its projections for future hadron colliders*

To complement the theoretical constraints, we also analyze the experimental measurements from LHC and its projections for the HL-LHC and HE-LHC. For a decay $S \rightarrow X$ or a production process $\sigma(pp \rightarrow S)$, the signal strength is defined as

$$\mu_X = \frac{\sigma(pp \rightarrow h) \cdot \mathcal{BR}(h \rightarrow X)}{\sigma(pp \rightarrow h^{\text{SM}}) \cdot \mathcal{BR}(h^{\text{SM}} \rightarrow X)}, \quad (2.13)$$

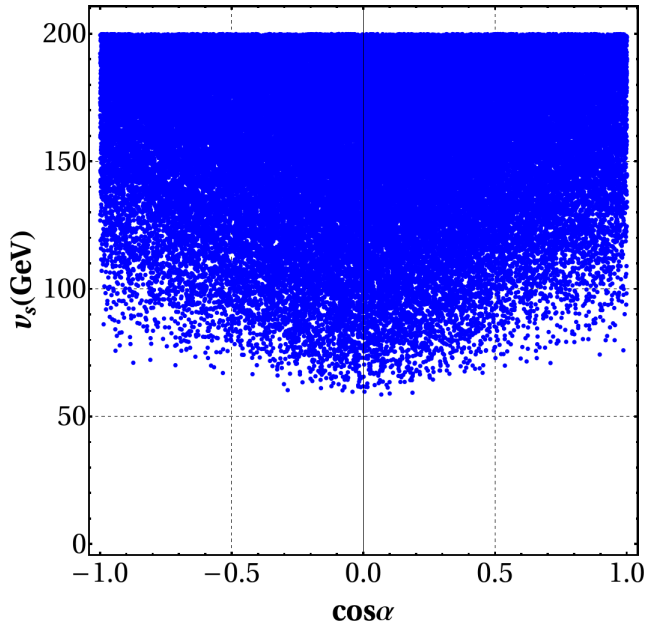


FIG. 1: Parameter space in the $\cos \alpha - v_s$ plane. Blue points stand for these that satisfy all the theoretical constraints.

where $\sigma(pp \rightarrow S)$ is the production cross section of S , with $S = h, h^{\text{SM}}$; here h is the SM-like Higgs boson coming from an extension of the SM and h^{SM} is the SM Higgs boson; $\mathcal{BR}(S \rightarrow X)$ is the branching ratio of the decay $S \rightarrow X$, where $X = c\bar{c}, b\bar{b}, \tau^-\tau^+, \mu^-\mu^+, WW^*, ZZ^*, \gamma\gamma$. In our analysis of μ_X , we consider $\tilde{Z}_{bb} = 0.01$ and $\tilde{Z}_{tt} = 0.4$. Such values are well motivated because they simultaneously accommodate all the μ_X 's. In fact, values in the $0.01 \leq \tilde{Z}_{bb} \leq 0.1$ and $0.1 \leq \tilde{Z}_{tt} \leq 1$ intervals have no important impact on the μ_X 's. However, in the case $\tilde{Z}_{bb} \geq 0.1$ and $\tilde{Z}_{tt} \geq 2$, a large reduction of allowed values in the $\cos \alpha - v_s$ plane is found.

4. Lepton Flavor-Violating processes

Furthermore, we also analyze lepton flavor-violating processes that can help us to complement the model parameter space in the $\cos \alpha - v_s$ plane. The processes considered for that aim are i) upper limits on the $\mathcal{BR}(\mu \rightarrow e\gamma), \mathcal{BR}(\tau \rightarrow \mu\gamma), \mathcal{BR}(\tau \rightarrow e\gamma)$, ii) upper limits on $\mathcal{BR}(\mu \rightarrow 3e), \mathcal{BR}(\tau \rightarrow 3e), \mathcal{BR}(\tau \rightarrow 3\mu)$ and $\mathcal{BR}(\mu \rightarrow \mu ee)$, iii) measurements of the $\mathcal{BR}(B_s \rightarrow \mu\mu)$ and $\mathcal{BR}(B_d \rightarrow \mu\mu)$ and finally iv) muon anomalous magnetic moment δa_μ . The processes i)-iii) are not very restrictive in the FNSM. This is mainly because of the choice we made for the matrix elements $\tilde{Z}_{\mu\mu}$ and $\tilde{Z}_{\tau\tau}$, as they play a subtle role in the couplings (see Tab. I) $\phi\mu\mu$ and $\phi\tau\tau$ ($\phi = h, H_F, A_F$), which have a significant impact on the observables $\tau \rightarrow 3\mu, \tau \rightarrow \mu\gamma, \mu \rightarrow e\gamma$. In fact, we consider $\tilde{Z}_{\tau\tau} = 0.2$ and $\tilde{Z}_{\mu\mu} = 10^{-4}$ (hence, a strong hierarchy), otherwise the SM $h\mu\mu$

coupling would be swamped by corrections from the FNSM. In contrast, we find that the most stringent constraint comes from δa_μ , which imposes an upper limit on the complex singlet VEV v_s . However, the situation could change because it is still possible that more precise determinations of the SM hadronic contribution and the experimental measurement would settle the discrepancy in the future without requiring any new physics effects. Thus, in this work we remain conservative but with an open stance to the above described happening.

We present in Fig. 2 the most restrictive observables of the model parameter space, limitedly to the reduced intervals $-1 \leq \cos \alpha \leq -0.95$ and $0.95 \leq \cos \alpha \leq 1$ since it is the region in which all the analyzed observables converge.

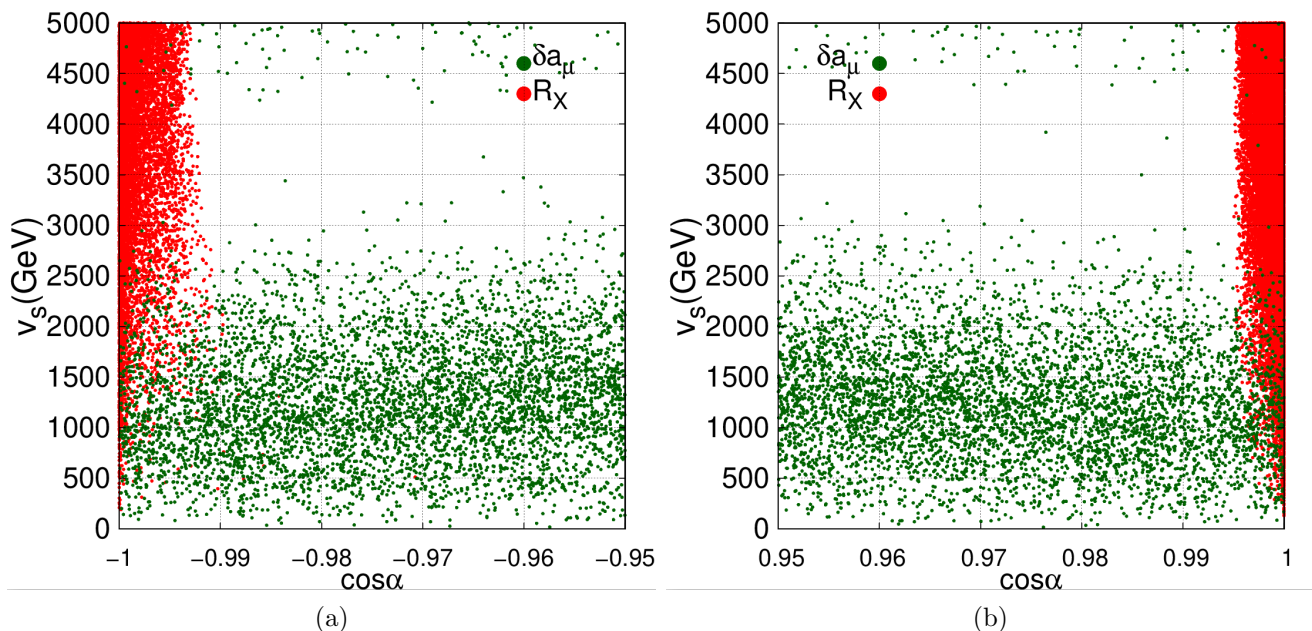


FIG. 2: Allowed region by all the constraints studied in the $\cos \alpha - v_s$ plane. (a) Interval limited $-1 \leq \cos \alpha \leq -0.95$ and (b) Interval limited $0.95 \leq \cos \alpha \leq 1$. Red points correspond to those allowed by all the μ_X 's, while the green points represent to those allowed by δa_μ .

It is important to mention that quark flavor constraints, namely, $B - \bar{B}$ mixing, $K - \bar{K}$ mixing and $D - \bar{D}$ mixing might impose severe restrictions on some model parameters. In Ref. [16, 22] this is made evident on the $M_{AF} - v_s$ plane, which strictly bounds M_{AF} as a function of v_s . We avoid these dangerous bounds via the deletion of the matrix elements \tilde{Z}_{db} , \tilde{Z}_{ds} and \tilde{Z}_{uc} (see Table I) for $B - \bar{B}$ mixing, $K - \bar{K}$ mixing, $D - \bar{D}$ mixing, respectively. To make this clear, we present in Fig. 3 the $M_{HF} - v_s$ plane for three different values of \tilde{Z}_{uc} ; 10^{-10} , 10^{-9} and 5×10^{-9} . The colored areas are these allowed by $|M_{12}^D|$ [23].

$$|M_{12}^D| < 7.5 \times 10^{-3} \text{ ps}^{-1} . \quad (2.14)$$

Similar constraints are obtained for $K - \bar{K}$ and $B - \bar{B}$.

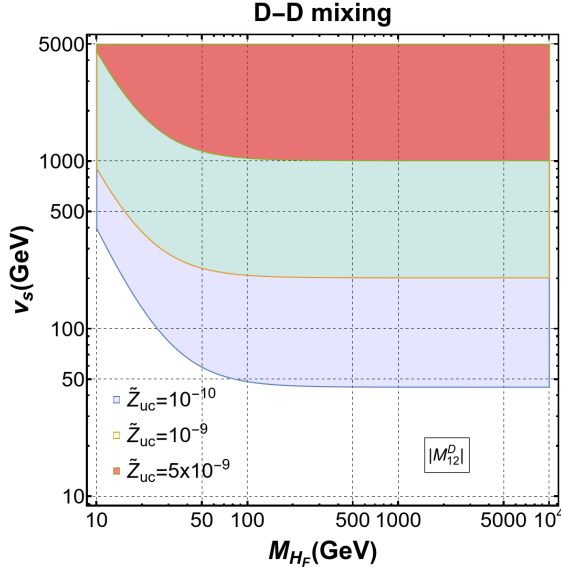


FIG. 3: $M_{HF} - v_s$ plane showing the region allowed due to flavon contributions to $|M_{12}^D|$. Blue area: $\tilde{Z}_{uc}=10^{-10}$, green area: $\tilde{Z}_{uc}=10^{-9}$, red area: $\tilde{Z}_{uc}=5 \times 10^{-9}$.

In conclusion, we define four benchmark points (BMP) to be used in the simulations in the next section.

- BMP1: $v_s = 301$ GeV, $\cos \alpha = 0.998$,
- BMP2: $v_s = 353$ GeV, $\cos \alpha = -0.997$,
- BMP3: $v_s = 888$ GeV, $\cos \alpha = -0.999$,
- BMP4: $v_s = 191$ GeV, $\cos \alpha = -0.999$.

III. COLLIDER ANALYSIS

This section presents a compressive study on the signal and SM background processes. We also present the strategy for separating one from the other. Explicit analytic expressions for the production mechanism of the flavon and its decay into photons are also presented.

Production and decay of the flavon

We are interested in the production of the CP-even flavon H_F , the dominant mechanism for producing it is via gluon fusion. This interaction can be extracted through the Lagrangian:

$$\mathcal{L}_{\text{eff}} = \frac{1}{v} g_{hgg} h G_{\mu\nu} G^{\mu\nu}, \quad (3.1)$$

$$g_{Sgg} = -i \frac{\alpha_S}{8\pi} \tau (1 + (1 - \tau) f(\tau)) \quad \text{with} \quad \tau = \frac{4M_t^2}{M_h^2}, \quad (3.2)$$

$$f(\tau) = \begin{cases} (\sin^{-1} \sqrt{\frac{1}{\tau}})^2, & \tau \geq 1, \\ -\frac{1}{4} [\ln \frac{1+\sqrt{1-\tau}}{1-\sqrt{1-\tau}} - i\pi]^2 & \tau < 1. \end{cases} \quad (3.3)$$

In FNSM, the ggh , ggH_F and ggA_F couplings are given, respectively, by:

$$g_{hgg} = \left(\frac{c_\alpha v_s - s_\alpha v}{v_s} \right) g_{Sgg} \quad (3.4)$$

$$g_{H_F gg} = \left(\frac{c_\alpha v + s_\alpha v_s}{v_s} \right) g_{Sgg} \quad (3.5)$$

$$g_{A_F gg} = \frac{v}{v_s} (-i \alpha_S / \pi) \tau f(\tau) \quad (3.6)$$

We present in Fig. 4 the production cross section of the flavon H_F as a function of its mass for the colliders: HL-LHC ($\sqrt{s} = 14$ TeV), HE-LHC ($\sqrt{s} = 27$ TeV), FCC-hh ($\sqrt{s} = 100$ TeV), and the BMPs defined in Sec. II C 4. The most optimistic case for producing flavons is BMP4, which predicts cross sections (at $\sqrt{s} = 14$ TeV), from 200 to 10^4 fb, corresponding to the range of masses 200 – 1000 GeV. In contrast, the least favored scenario is BMP3. The cross section of this scenario range from 8 fb to 500 fb for $M_{H_F} = 1000, 200$, respectively. These values are expected because the singlet complex VEV v_s suppresses the FNSM correction of the flavon production via gluon fusion, as shown in Eq. (3.5). For $\sqrt{s} = 27, 100$ TeV, the cross sections are up to 1 and 2 orders of magnitude larger than 14 TeV, respectively.

On the other hand, we also need to know the branching ratio of the decay $H_F \rightarrow \gamma\gamma$, which can be obtained with the following expression:

$$\Gamma(H_F \rightarrow \gamma\gamma) = \frac{\alpha^2 M_{H_F}^3}{1024 \pi^3 m_W^2} \left| \sum_s A_s^{H_F \gamma\gamma}(\tau_s) \right|^2, \quad (3.7)$$

where the subscript $s = 0, 1/2, 1$ refers to the spin of the charged particle circulating in the loop,

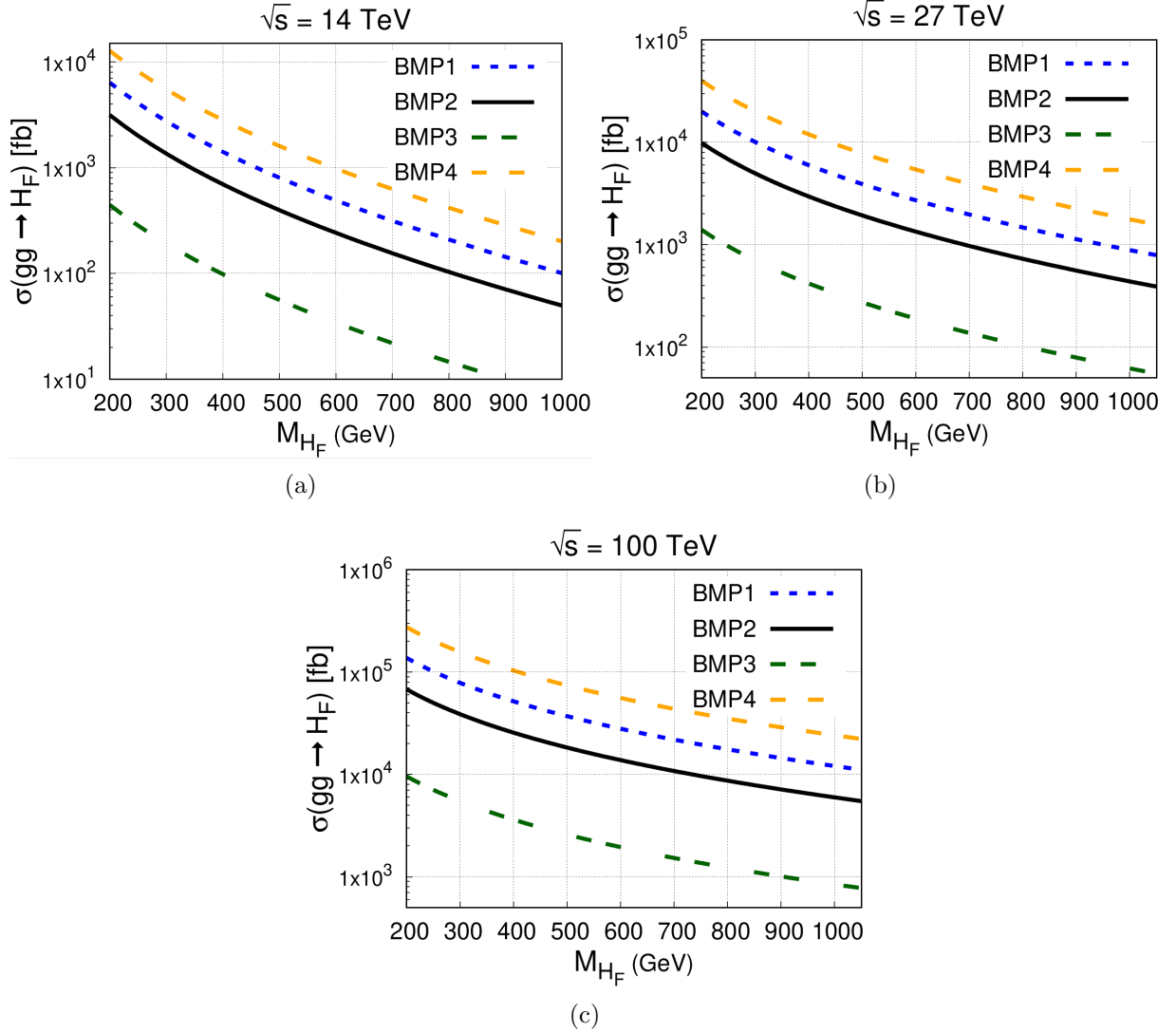


FIG. 4: Production cross-section of the flavon via gluon fusion in pp collisions $\sigma(gg \rightarrow H_F)$. (a) For the HL-LHC at $\sqrt{s} = 14$ TeV, (b) For the HE-LHC at $\sqrt{s} = 27$ TeV, (c) For the FCC-hh at $\sqrt{s} = 100$ TeV.

and

$$A_s^{H_F\gamma\gamma} = \begin{cases} \sum_f \frac{2m_W g_{H_F f_i \bar{f}_i} N_c Q_f^2}{m_f} \left[-2\tau_s (1 + (1 - \tau_s) f(\tau_s)) \right] & \text{for } s = \frac{1}{2}, \\ g_{H_F WW} \left[2 + 3\tau_W + 3\tau_W (2 - \tau_W) f(\tau_W) \right] & \text{for } s = 1, \end{cases} \quad (3.8)$$

where

$$f(x) = \begin{cases} \arcsin^2\left(\frac{1}{\sqrt{x}}\right), & x \geq 1, \\ -\frac{1}{4} \left[\log\left(\frac{1+\sqrt{1-x}}{1-\sqrt{1-x}}\right) - i\pi \right]^2, & x < 1. \end{cases} \quad (3.9)$$

and $N_c = 1, 3$ for leptons and quarks, respectively, $\tau_a = 4M_a^2/M_{H_F}^2$. The couplings $g_{H_F f_i \bar{f}_i}$ and $g_{H_F WW}$ are given in Table I. Figure 5 shows the $\mathcal{BR}(H_F \rightarrow \gamma\gamma)$ as a function of the flavon mass M_{H_F} for the BMPs defined in Sec. II C 4.

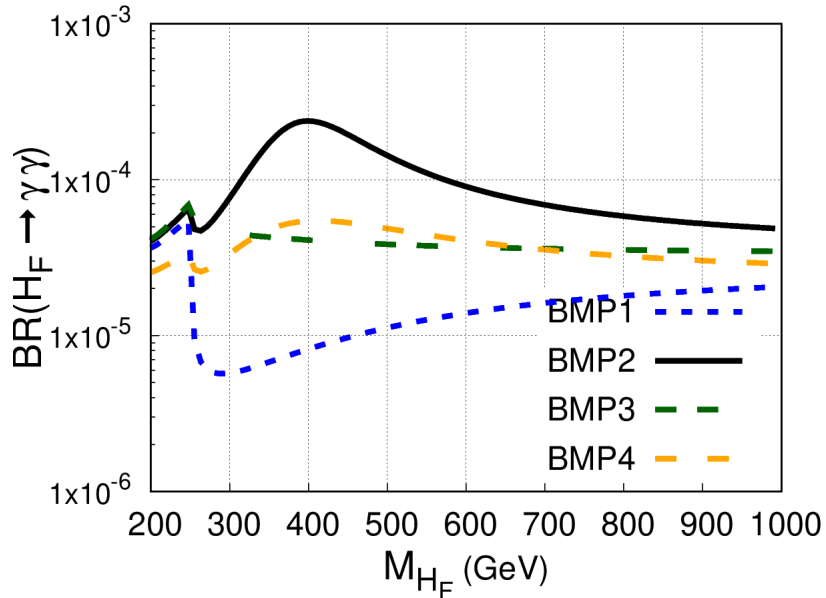


FIG. 5: Branching ratio $\mathcal{BR}(H_F \rightarrow \gamma\gamma)$ as a function of the Flavon mass M_{H_F} .

According to our analysis of the FNSM parameter space, branching ratios from $\mathcal{O}(10^{-6})$ to $\mathcal{O}(10^{-4})$ can be obtained, for BMP2 ($M_{H_F} \sim 400$ GeV) and BMP1 ($M_{H_F} \sim 250$ GeV), respectively; while for BMP3 and BMP4 we obtain similar branching ratios for the range $320 \leq M_{H_F} \leq 1000$ GeV. The discontinuous behavior in all BMPs is due to several factors, the most distinctive being the emergence or suppression of different flavon decay channels. In particular, once $M_{H_F} \sim 250$ GeV, there is an inflection point associated with the emergence of the $H_F \rightarrow hh$ di-Higgs channel. For $M_{H_F} > 1000$ GeV, the $\mathcal{BR}(H_F \rightarrow \gamma\gamma)$ converges to a value of order 10^{-5} . The values of the branching ratios are relatively high due to the BMPs defined for our study. From Eq. (3.8) and Table I, we notice that $\mathcal{BR}(H_F \rightarrow \gamma\gamma) \sim 1/v_s$, with v_s being of order 10^2 in the BMPs defined, it suppresses the $\mathcal{BR}(H_F \rightarrow \gamma\gamma)$ by a factor of 10^{-2} with respect to the $\mathcal{BR}(h \rightarrow \gamma\gamma)$ of the SM, which is of order 10^{-3} . Thus, the $\mathcal{BR}(H_F \rightarrow \gamma\gamma)$ shown in Fig. 5 are reasonable and motivate

their possible experimental scrutiny.

Signal and background

- *Signal:* We search for a final state $\gamma\gamma$ generated by the decay $H_F \rightarrow \gamma\gamma$, where the flavon H_F is produced by gluon fusion. The analysis is performed in the mass range of 200-1000 GeV. We present in Fig. 6 the Feynman diagram of the signal. While Fig. 7 shows the production cross section $\sigma(gg \rightarrow H_F \rightarrow \gamma\gamma)$ (left vertical axis) and the number of events produced (right vertical axis) as a function of M_{H_F} .

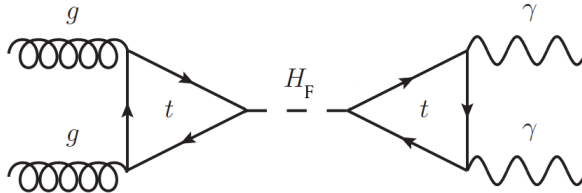


FIG. 6: Feynman diagram of the signal $gg \rightarrow H_F \rightarrow \gamma\gamma$.

- *Background:* The dominant irreducible background is the SM di-photon production ($\gamma\gamma$); contributions also come from $\gamma + j$ and $j + j$ production with one or two jets misidentified as photons and from the Drell-Yan process.

Event selection

The identification of the signal depends mainly on the true p_T^γ of the photons. The photon selection efficiency as a function of the p_T^γ of the true photon is parametrised by

$$\epsilon(p_T^\gamma) = 0.76 - 1.98 \times e^{-\frac{p_T^\gamma}{16.1\text{GeV}}}. \quad (3.10)$$

On the other hand, the rate of jets passing the photon identification and isolation requirements can be identified as fake photons. The rate is parametrised as a function of the true jet p_T^j via :

$$\epsilon(p_T^j) = 9.3 \cdot 10^{-3} \times e^{-\frac{p_T^j}{27.5\text{GeV}}}. \quad (3.11)$$

The strategy to isolate the signal from the background is to impose the criteria in Eqs. (3.10)-(3.11) and to perform a Boosted Decision Trees (BDT) training [24] by using variables related to the kinematics of the final state. Table III shows the variables used to train and test the signal

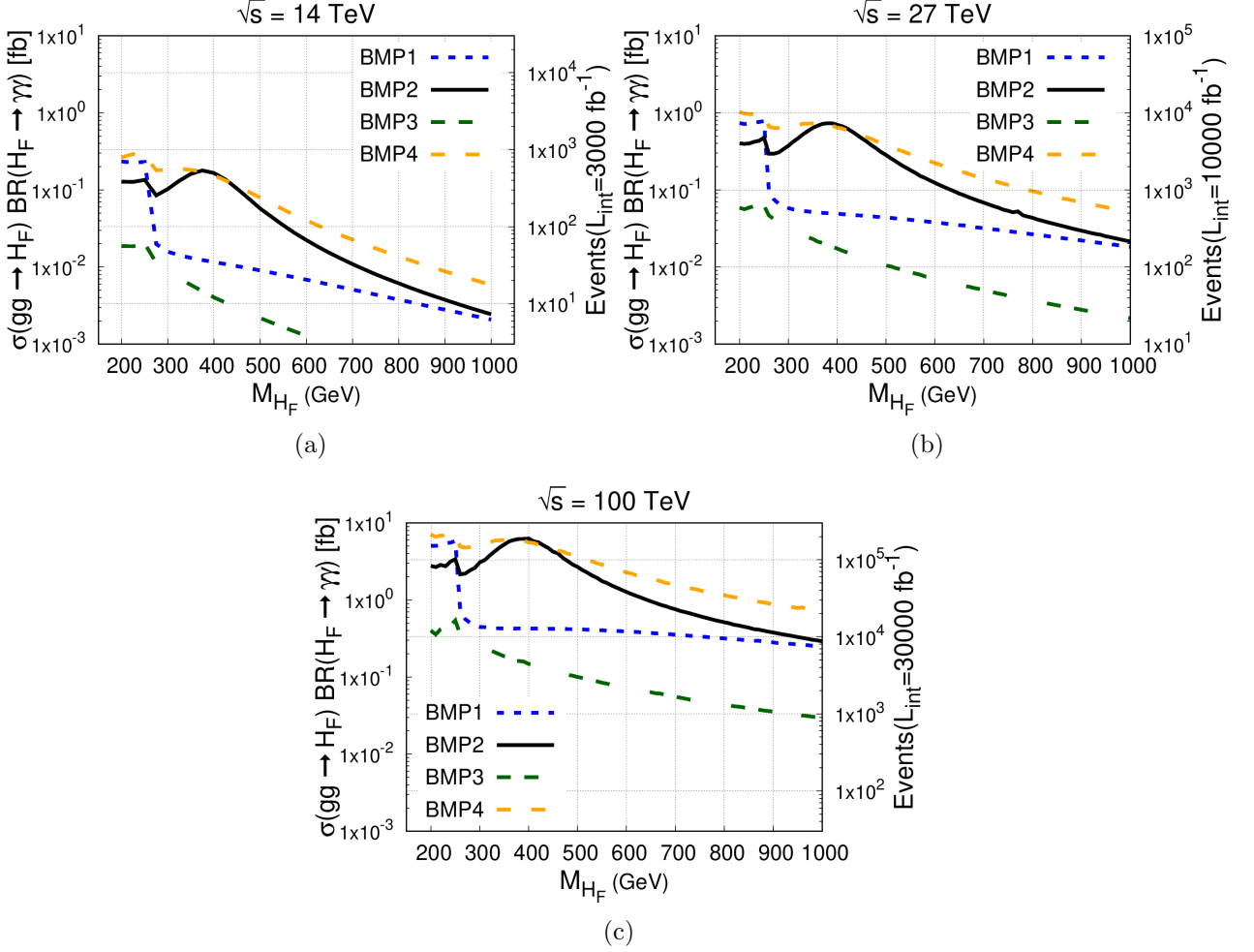


FIG. 7: On the left vertical axis: Production cross-section $\sigma(pp \rightarrow H_F \rightarrow \gamma\gamma)$ as a function of the Flavon mass M_{H_F} . On the right vertical axis: Number of events produced as a function of the Flavon mass M_{H_F} .

and background events. According to our analysis, the most discriminating observables are the transverse momentum of the leading photon $p_T^{\gamma_1}$ and the invariant mass $M_{\text{inv}}(\gamma\gamma)$. We show in Fig. 8 these distributions for $M_{H_F} = 400$ GeV. Meanwhile, Fig. 9 presents the discriminant for the signal and background. The goodness of fit is checked via the Kolmogorov-Smirnov (KS) test. Our analysis shows that the KS value is within the permissible $[0, 1]$ interval, namely, 0.29 and 0.91 for the background and the signal, respectively. The relevant hyperparameters for the BDT training are as follows: Number of trees $N_{\text{Tree}}=110$, maximum depth of the decision tree $\text{MaxDepth}=4$, maximum number of leaves $\text{MaxLeaves}=14$. The training is performed using the MC-simulated samples. These signal and background samples are scaled to the expected number of candidates, which is calculated based on the integrated luminosity and cross sections. The BDT selection is

TABLE III: List of the variables used to train and test the signal and background events.

Rank	Variable	Description
1	$p_T^{\gamma_1}$	Photon with the largest transverse momentum.
2	$M_{\text{inv}}(\gamma\gamma)$	Invariant mass
3	$N(j)$	Number of jets
4	ΔR	The R separation between the photons
5	$p_T^{\gamma_2}$	Transverse momentum of the subleading photon
6	η_1	Pseudorapidity of the leading photon
7	η_2	Pseudorapidity of the subleading photon
8	$\phi(\gamma_1)$	Azimuth angle of the leading photon
9	$\phi(\gamma_2)$	Azimuth angle of the subleading photon

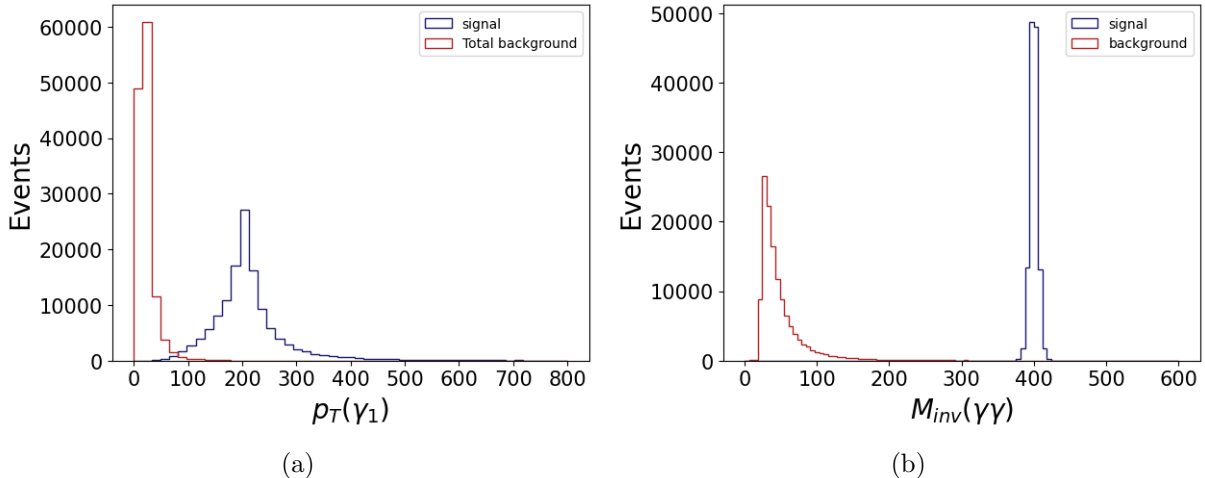


FIG. 8: (a) Transverse momentum of the leading photon $p_T^{\gamma_1}$, (b) Invariant mass $M_{\text{inv}}(\gamma\gamma)$ for $M_{H_F} = 400$ GeV.

optimized individually for each flavon mass M_{H_F} to maximize the figure of merit, i.e., the *signal significance*, defined as $S/\sqrt{S+B}$, where S and B represent the number of signal and background candidates, respectively, in the signal region after applying the selection criteria.

Figure 10 presents contour plots of the *signal significance* as a function of the flavon mass M_{H_F} and the integrated luminosity for the BMP2. In particular, we obtain *signal significances* at the level of 5σ for $350 \lesssim M_{H_F} \lesssim 450$ GeV and $200 \leq M_{H_F} \leq 1000$ GeV for the HE-LHC and FCC-hh, respectively. The least favored scenario is for the HL-LHC, which does not provide the ease of detection of the flavon. Similarly, Fig 11 presents the *signal significance* for the benchmark point BMP4 with similar results for the HL-LHC. However, this scenario provides a range of masses that could be detected slightly greater than the previous case. Specifically, the HE-LHC offers

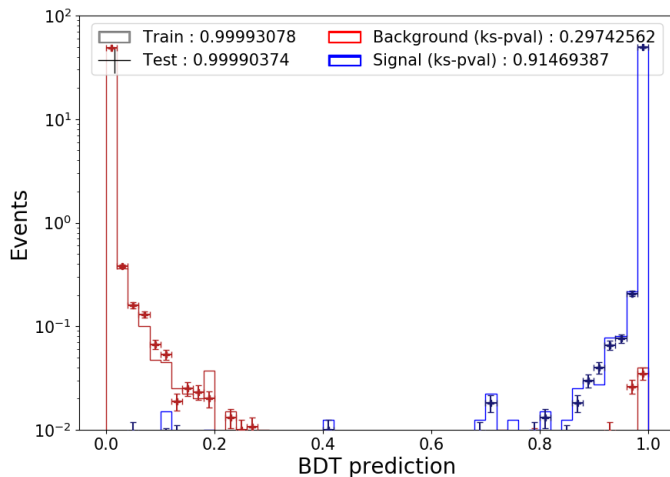


FIG. 9: Plot of the discriminant for signal and background data.

the possibility of detection of the flavon in the range of masses $200 - 450$ GeV. More encouraging results appear at FCC-hh, achieving a potential discovery in a wider range of masses, covering the entire mass spectrum studied in this paper. In contrast, for the least hopeful case, BMP3, we found a maximum significance of 2.12σ for the FCC-hh by considering its final integrated luminosity and $M_{H_F} = 200$ GeV. As far as BMP1 is concerned, we find results that approach an intermediate case of BMPs 2 and 3 for $400 \lesssim M_{H_F} \lesssim 600$ GeV and significances similar to BMP2 for $750 \lesssim M_{H_F} \lesssim 1000$. The most relevant *signal significances* for the BMP1, even at the level of the most optimistic BMPs (2 and 4), lie in the mass interval $200 \leq M_{H_F} \leq 250$.

IV. CONCLUSIONS

In this paper, we have studied the production of the so-called flavon H_F , with its subsequent decay into two photons (signal). The flavon is a hypothetical particle predicted in a model that invokes the Froggatt-Nielsen mechanism, which is the theoretical framework considered in this paper. The mechanism of production of the flavon is via proton-proton collisions at super hadron colliders, namely: High-Luminosity LHC, High-Energy LHC and the Future hadron-hadron Circular Collider. To give realistic predictions, we test the free parameters of the model against theoretical and experimental constraints and then we define benchmark points (BMPs) to perform Monte Carlo simulations. The most severe constraint on the cosine of the mixing angle ($\cos \alpha \sim -1$ or ~ 1) that mixes the neutral and real parts of the Higgs doublet and the complex singlet with the physical fields h and H_F comes from the LHC Higgs boson data and their projections for the HE-LHC. This is expected in order to avoid dangerous corrections to the Higgs boson couplings to fermions

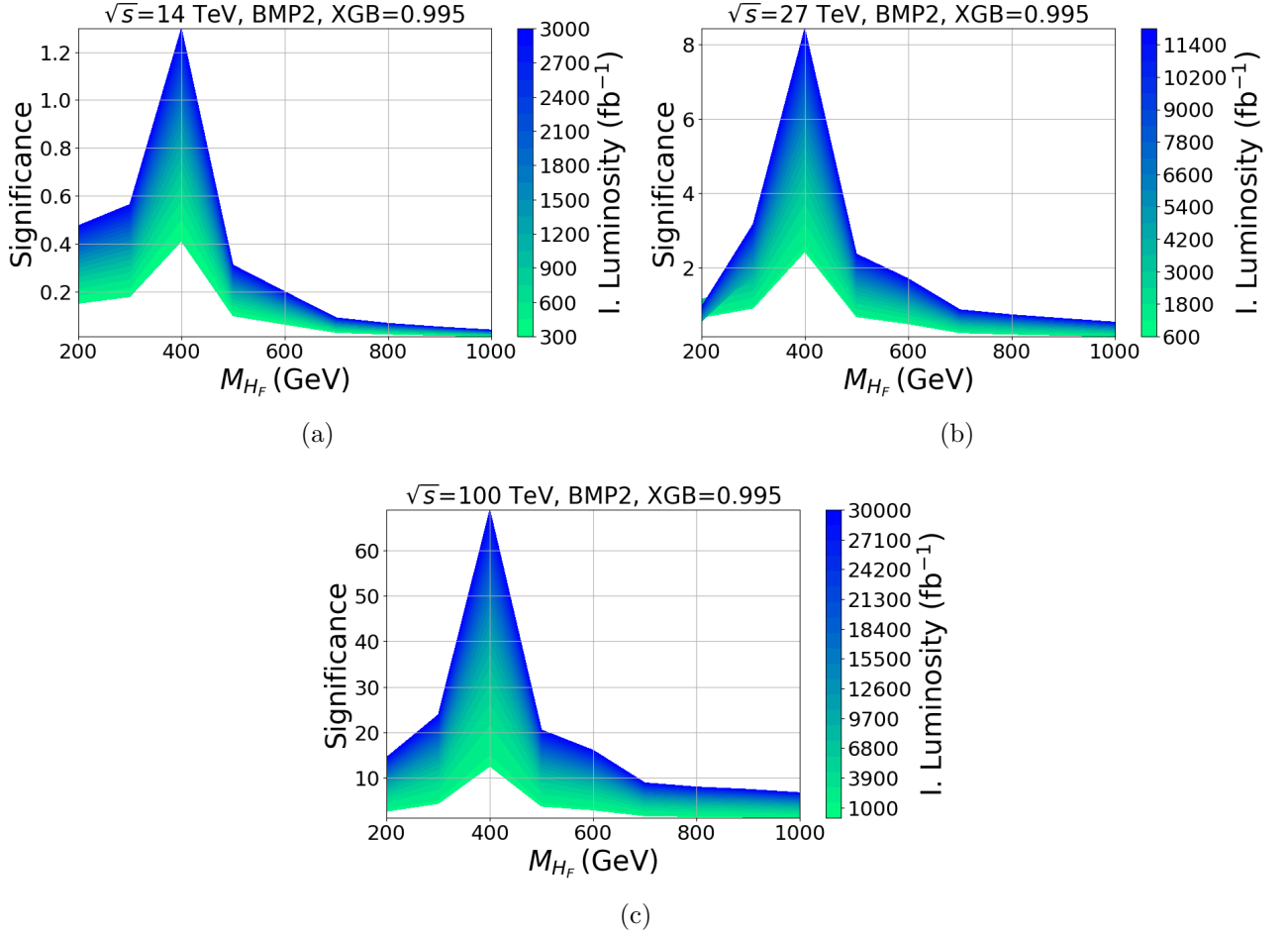


FIG. 10: Significance as a function of the flavon mass M_{H_F} and the integrated luminosity, for the BMP2. (a) HL-LHC, (b) HE-LHC and (c) FCC-hh. In all the cases we impose a cut on the BDT prediction $XGB=0.995$.

and gauge bosons. As far as the VEV of the complex singlet v_s is concerned, the muon anomalous magnetic moment is the most restrictive observable on v_s , allowing $v_s \lesssim 3$ TeV. However, the situation could change because it is still possible that more precise determinations of the SM hadronic contribution and the experimental measurement would settle the discrepancy in the future without requiring any new physics effects. Thus, in this work we remain conservative but with an open stance to the above described happening.

On the other hand, based on the defined BMPs, and using events simulated for the signal and its SM background, we perform an analysis with machine learning via the Boosted Decision Trees method to isolate the signal from the background. We find that the nearest evidence could emerge at the HE-LHC with a *signal significance* of 5σ for integrated luminosities in the range $5 - 12 \text{ ab}^{-1}$ and flavon masses between $350 - 450$ GeV ($200 - 450$) for the BMP2 (BMP4). These

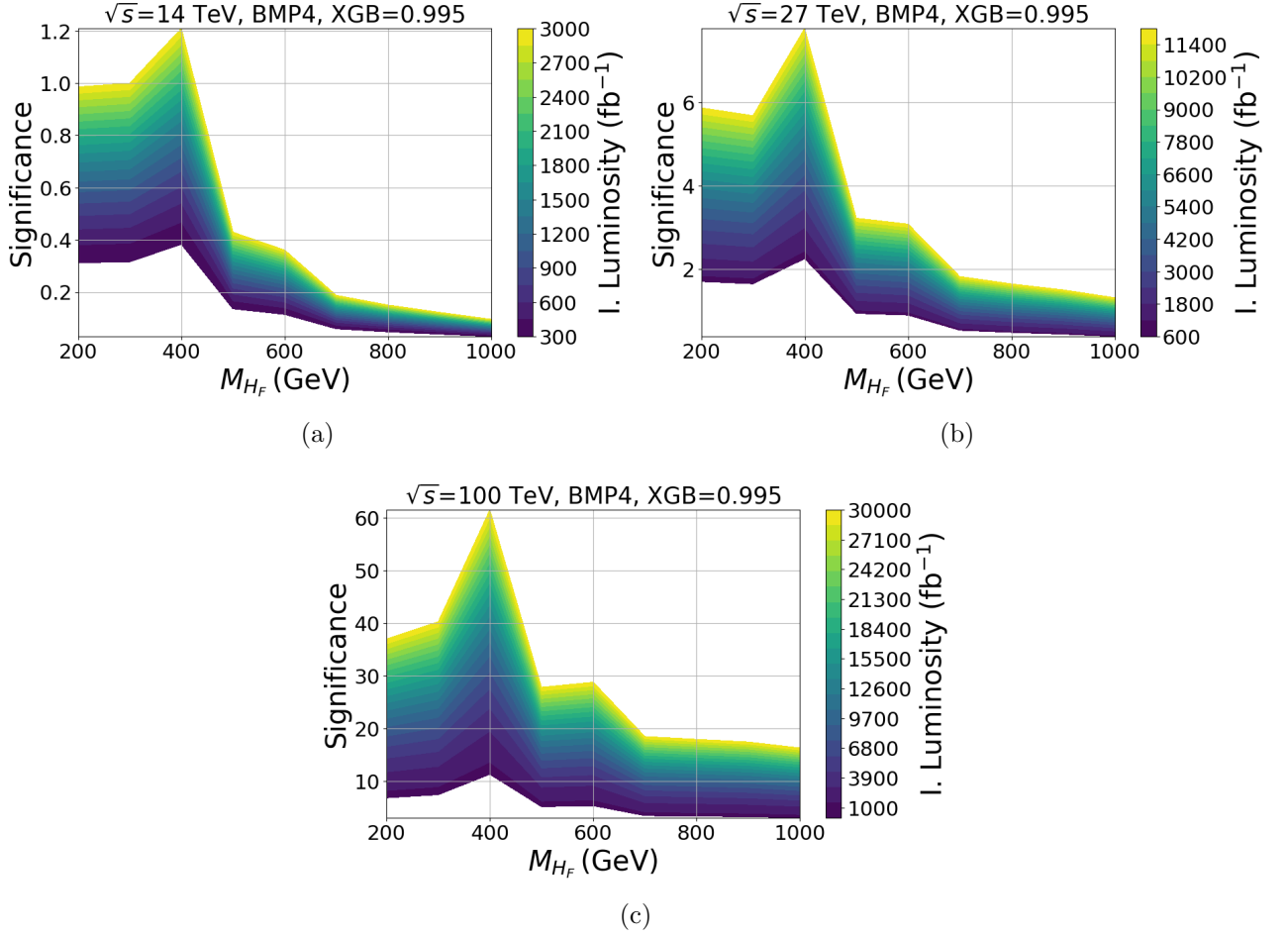


FIG. 11: Significance as a function of the flavon mass M_{H_F} and the integrated luminosity, for the BMP4. (a) HL-LHC, (b) HE-LHC and (c) FCC-hh. In all the cases we impose a cut on the BDT prediction XGB=0.995.

predictions could be corroborated in the Future hadron-hadron Circular Collider. Furthermore, this collider would have the capability to search for broader range of masses, covering the entire interval studied in this work. Thus, we predict *signal significances* at the level of 5σ for the range $200 \leq M_{H_F} \leq 1000$ GeV. Even more, projecting our results, the FCC-hh might be able to search for flavon masses as high as 5 TeV.

ACKNOWLEDGEMENTS

The work of Marco A. Arroyo-Ureña and T. Valencia-Pérez is supported by “Estancias Posdoctorales por México (SECIHTI)” and “Sistema Nacional de Investigadores” (SNI-SECIHTI). T.V.P. acknowledges support from the UNAM project PAPIIT IN111224 and the SECIHTI project

-
- [1] S. L. Glashow. Partial Symmetries of Weak Interactions. *Nucl. Phys.*, 22:579–588, 1961.
- [2] Steven Weinberg. A Model of Leptons. *Phys. Rev. Lett.*, 19:1264–1266, 1967.
- [3] Abdus Salam and John Clive Ward. Weak and electromagnetic interactions. *Nuovo Cim.*, 11:568–577, 1959.
- [4] Gerard 't Hooft and M. J. G. Veltman. Regularization and Renormalization of Gauge Fields. *Nucl. Phys. B*, 44:189–213, 1972.
- [5] T. W. B. Kibble. Symmetry breaking in nonAbelian gauge theories. *Phys. Rev.*, 155:1554–1561, 1967.
- [6] Peter W. Higgs. Broken Symmetries and the Masses of Gauge Bosons. *Phys. Rev. Lett.*, 13:508–509, 1964.
- [7] Peter W. Higgs. Spontaneous Symmetry Breakdown without Massless Bosons. *Phys. Rev.*, 145:1156–1163, 1966.
- [8] G. S. Guralnik, C. R. Hagen, and T. W. B. Kibble. Global Conservation Laws and Massless Particles. *Phys. Rev. Lett.*, 13:585–587, 1964.
- [9] Peter W. Higgs. Broken symmetries, massless particles and gauge fields. *Phys. Lett.*, 12:132–133, 1964.
- [10] F. Englert and R. Brout. Broken Symmetry and the Mass of Gauge Vector Mesons. *Phys. Rev. Lett.*, 13:321–323, 1964.
- [11] Georges Aad et al. Observation of a new particle in the search for the Standard Model Higgs boson with the ATLAS detector at the LHC. *Phys. Lett.*, B716:1–29, 2012.
- [12] Serguei Chatrchyan et al. Observation of a new boson with mass near 125 GeV in pp collisions at $\sqrt{s} = 7$ and 8 TeV. *JHEP*, 06:081, 2013.
- [13] C. D. Froggatt and Holger Bech Nielsen. Hierarchy of Quark Masses, Cabibbo Angles and CP Violation. *Nucl. Phys. B*, 147:277–298, 1979.
- [14] M. A. Arroyo-Ureña, J. L. Díaz-Cruz, G. Tavares-Velasco, A. Bolaños, and G. Hernández-Tomé. Searching for lepton flavor violating flavon decays at hadron colliders. *Phys. Rev. D*, 98(1):015008, 2018.
- [15] Marco A. Arroyo-Ureña, Amit Chakraborty, J. Lorenzo Díaz-Cruz, Dilip Kumar Ghosh, Najimuddin Khan, and Stefano Moretti. Flavon signatures at the HL-LHC. *Phys. Rev. D*, 108(9):095026, 2023.
- [16] Gauhar Abbas, Ashutosh Kumar Alok, Neetu Raj Singh Chundawat, Najimuddin Khan, and Neelam Singh. Finding flavons at colliders. *Phys. Rev. D*, 110(11):115015, 2024.

- [17] Amit Chakraborty, Dilip Kumar Ghosh, Najimuddin Khan, and Stefano Moretti. Exploring the Dark Sector of the inspired FNSM at the LHC. 5 2024.
- [18] G. Apollinari, O. Brüning, T. Nakamoto, and Lucio Rossi. High Luminosity Large Hadron Collider HL-LHC. *CERN Yellow Rep.*, (5):1–19, 2015.
- [19] Michael Benedikt and Frank Zimmermann. Proton Colliders at the Energy Frontier. *Nucl. Instrum. Meth. A*, 907:200–208, 2018.
- [20] Nima Arkani-Hamed, Tao Han, Michelangelo Mangano, and Lian-Tao Wang. Physics opportunities of a 100 TeV proton–proton collider. *Phys. Rept.*, 652:1–49, 2016.
- [21] Najimuddin Khan and Subhendu Rakshit. Study of electroweak vacuum metastability with a singlet scalar dark matter. *Phys. Rev. D*, 90(11):113008, 2014.
- [22] Martin Bauer, Torben Schell, and Tilman Plehn. Hunting the Flavon. *Phys. Rev. D*, 94(5):056003, 2016.
- [23] A. J. Bevan et al. The utfit collaboration average of d meson mixing data: Winter 2014. *JHEP*, 1403:123, 2014.
- [24] L. Breiman et al. *Classification and regression trees*. Wadsworth international group, California, USA, 1984.